Reconciling Kubo and Keldysh Approaches to Fermi-Sea-Dependent Nonequilibrium Observables: Application to Spin Hall Current and Spin-Orbit Torque in Spintronics

Simão M. João,[1] Marko D. Petrović,[2] J. M. Viana Parente Lopes,[3] Aires Ferreira,[4,*] and Branislav K. Nikolić[2,†]

[1] *Department of Materials, Imperial College London, London SW7 2AZ, UK*
[2] *Department of Physics and Astronomy, University of Delaware, Newark, DE 19716, USA*
[3] *Centro de Física das Universidades do Minho e Porto and Departamento de Física e Astronomia, Faculdade de Ciências, Universidade do Porto, 4169-007 Porto, Portugal*
[4] *Department of Physics, University of York, YO10 5DD, York, UK*

Quantum transport studies of spin-dependent phenomena in solids commonly employ the Kubo or Keldysh formulas for the nonequilibrium density operator in the steady-state linear-response regime. Its trace with operators of interest, such as the spin density, spin current density, etc., gives expectation values of experimentally accessible observables. For local quantities, these formulas require summing over the manifolds of *both* Fermi-surface and Fermi-sea states. However, debates have been raging in the literature about the vastly different physics the two formulations can apparently produce, even when applied to the same system. Here, we revisit this problem using infinite-size graphene with proximity-induced spin-orbit and magnetic exchange effects as a testbed. By splitting this system into semi-infinite leads and central active region, in the spirit of Landauer formulation of quantum transport, we prove the *numerically exact equivalence* of the Kubo and Keldysh approaches via the computation of spin Hall current density and spin-orbit torque in both clean and disordered limits. The key to reconciling the two approaches are the numerical frameworks we develop for: (*i*) evaluation of Kubo(-Bastin) formula for a system attached to semi-infinite leads, which ensures continuous energy spectrum and evades the need for commonly used phenomenological broadening introducing ambiguity; and (*ii*) proper evaluation of Fermi-sea term in the Keldysh approach, which *must* include the voltage drop across the central active region even if it is disorder free.

The density (or state or statistical) operator [1] is the central concept of quantum statistical mechanics. The operator and its representation—the density matrix—in some basis of the Hilbert space is *sine qua non* to describe equilibrium quantum systems at finite temperature [2], as well as out-of-equilibrium systems driven by steady or time-dependent external fields. The density operator also plays a crucial role in describing the transition between nonequilibrium and equilibrium states [3], as well as in zero-temperature quantum mechanics [4] and quantum information science where it describes decoherence (i.e., the decay of the off-diagonal elements of the density matrix in some preferred basis [5]), and eventually quantum-to-classical transitions [5, 6]. From the knowledge of the density matrix $\hat{\rho}$, the expectation value of a physical observable represented by a Hermitian operator $\hat{O}$ is obtained from $O = \mathrm{Tr}\,[\hat{\rho}\hat{O}]$. The density matrix in equilibrium is unambiguously specified by the Boltzmann and Gibbs prescription. A textbook example [2] is the grand canonical ensemble $\hat{\rho}_{\rm eq} = \sum_n f(E_n)|E_n\rangle\langle E_n|$ for noninteracting fermions with single-particle energy levels E_n, occupied according to the Fermi-Dirac distribution function $f(E)$, and with the corresponding eigenstates $|E_n\rangle$ of a fermionic Hamiltonian. By contrast, there is no unique procedure to obtain the density matrix of steady-state [7, 8] or time-dependent [9–12] nonequilibrium systems and for arbitrary strength of the driving field [7], while including their many-body interactions [12].

Nonetheless, in problems of noninteracting electrons driven by weak external fields, linear-response theory of Kubo [13] or Keldysh Green's functions (GFs) [14, 15] makes it possible to construct a *universal* expression for $\hat{\rho}^{\rm neq}$ that is expressed in terms of the retarded GF involving Hamiltonian of the system in *equilibrium*, $\hat{H}$. For example, in the case of Kubo formula [13], and using Bastin *et. al.* [16] formulation in terms of GFs, the steady-state $\hat{\rho}^{\rm neq}$ (at zero temperature for simplicity) is given by

$$\hat{\rho}^{\rm neq}_{\rm Kubo} = \hat{\rho}^{\rm surf}_{\rm Kubo} + \hat{\rho}^{\rm sea}_{\rm Kubo}, \tag{1a}$$

$$\hat{\rho}^{\rm surf}_{\rm Kubo} = \frac{4eE_x}{h}\mathrm{Re}\left[\mathrm{Im}\,\hat{G}\,\hat{v}_{\rm x}\,\mathrm{Im}\,\hat{G}\right], \tag{1b}$$

$$\hat{\rho}^{\rm sea}_{\rm Kubo} = \frac{2eE_x}{h}\int dE f(E)\mathrm{Re}\left[(\hat{G}^r-\hat{G}^a)\hat{v}_{\rm x}\,\partial_E\mathrm{Re}\,\hat{G}\right], \tag{1c}$$

where $\partial_E \equiv \partial/\partial E$ and E_x is the strength of the small electric field (assumed to point along the $\hat{x}$-axis). Note that several decompositions [17] into $\hat{\rho}^{\rm sea}_{\rm Kubo}$ and $\hat{\rho}^{\rm surf}_{\rm Kubo}$, governed by the Fermi-sea and Fermi-surface states, respectively, have been used historically [18–22]. Here we employ the specific "symmetrized decomposition" of Ref. [21] ensuring no overlap between the two terms, while also using $\hat{\rho}^{\rm surf}_{\rm Kubo}$ as the Kubo-Greenwood form [23, 24] which is advantageous for comparison with Keldysh Eq. (4b). The retarded (r) GF standardly used in Eq. (1) is given by

$$\hat{G}^r = \left[E - \hat{H} + i\eta\right]^{-1}, \tag{2}$$

where $\hat{G}^a = (\hat{G}^r)^\dagger$ is the advanced GF; $\mathrm{Im}\,\hat{G} = (\hat{G}^r - \hat{G}^a)/2i$; $\mathrm{Re}\,\hat{G} = (\hat{G}^r+\hat{G}^a)/2$, $\hat{\mathbf{v}} = [\hat{\mathbf{r}}, \hat{H}]/i\hbar$ is the velocity operator and $\hat{\mathbf{r}}$ is the position operator. In most practical applications employing atomistic models [25, 26],

$\hat{H}$ is either a generic symmetry-allowed [27–30] or first-principles-derived [31–34] tight-binding Hamiltonian on a *finite* lattice with *periodic* boundary conditions. The parameter η (formally an infinitesimal) is required to define $\hat{G}^{r,a}$ by avoiding poles on the real axis [35], with the limit $\eta \to 0$ taken explicitly in analytical approaches [36–40]. However, in numerics η must remain nonzero due to the discreteness of energy levels [30, 41, 42], and it can be reduced only at the computational expense of handling larger systems or averaging over random twisted boundary conditions [43]. Physically, a finite η was initially interpreted as mimicking the effect of uncorrelated inelastic scattering processes, thereby defining a phenomenological dephasing timescale $\tau_\phi = \hbar/\eta$ [44]. Later on, η has often been interpreted [21, 31] as a homogeneous broadening due to scattering from short-range impurities, but disorder should be explicitly introduced as a term in $\hat{H}$ [such as through ε_i in Eq. (5)] in order to capture the same key concepts, disorder self-energy and vertex corrections, used in analytical calculations [36–40, 45]. Recently, inspired by the success of approximation theory [46, 47], a more practical and accurate interpretation has arisen, where η is seen as an energy resolution that determines how close finite-size spectral simulations are to describe genuine thermodynamic behavior [25, 48–50].

The Keldysh formalism [14, 15] is applicable beyond the linear-response regime by employing additional GFs. Its fundamental quantities are the retarded $\hat{G}^r(t,t')$ and the lesser $\hat{G}^<(t,t')$ GFs describing the density of available quantum states and how electrons occupy those states, respectively. The diagonal-in-time component of the latter yields the time-dependent nonequilibrium density matrix according to $\hat{\rho}^{\rm neq}_{\rm Keldysh}(t) = \frac{\hbar}{i}\hat{G}^<(t,t)$ [9]. In steady-state out-of-equilibrium scenarios, all quantities depend only on the difference $t-t'$, so that after a Fourier transformation in energy domain E, $\hat{G}^<(E)$ yields the Keldysh formula for the nonequilibrium density matrix, $\hat{\rho}^{\rm neq}_{\rm Keldysh} = \frac{1}{2\pi i}\int dE\, \hat{G}^<(E)$. This formula is widely used in computational quantum transport [51] studies of two- [52–56] or multi-terminal [57, 58] Landauer setups [23, 41, 51, 59–62], where a finite-length central active (CA) region, as in Fig. 1, is coupled to macroscopic Fermi liquid reservoirs via ideal semi-infinite leads. For instance, in the two-terminal geometry in which the left (L) and right (R) lead terminate into the corresponding reservoirs characterized by the Fermi-Dirac functions, $f_{L,R} = f(E-\mu_{L,R})$, and in the presence of a bias voltage $eV_b = \mu_L - \mu_R$ [here, $\mu_{L,R}$ denotes the electrochemical potential [63] of L or R lead], the lesser GF of the CA region was expressed by Caroli *et al.* [61] as $\hat{G}^<(E) = i\hat{G}^r(E)\left[f_L(E)\hat{\Gamma}_L(E) + f_R(E)\hat{\Gamma}_R(E)\right]\hat{G}^a(E)$. The simplicity of this expression stems from the assumption of many-body interactions being absent both in the CA region [64–66] and in the leads [67]. Here the

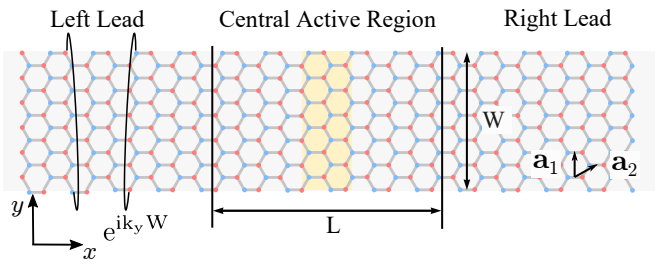

FIG. 1. Doubly-proximitized [70] infinite graphene sheet viewed as a two-terminal Landauer setup [23, 59–62] for computational quantum transport [51] with its CA region being an armchair nanoribbon (of finite length $L = 40$ Å and width $W = 15$ Å) attached to semi-infinite nanoribbons of the same kind. The nanoribbon is periodically repeated along the y-axis to reproduce bulk behavior of an infinite sheet [71]. We employ this setup in the calculation of SH current density [Fig. 2] and SO torque [Fig. 3], within the shaded-in-yellow middle strip, via both Kubo Eq. (1) and Keldysh Eq. (4).

retarded GF

$$\hat{G}^r(E) = \left[E - \hat{H} - \hat{\Sigma}^r_L(E) - \hat{\Sigma}^r_R(E)\right]^{-1}, \tag{3}$$

differs from Eq. (2) used in typical numerical Kubo calculations on systems with periodic boundary conditions [26, 27, 30–33, 58] as it incorporates the leads through their self-energies [51, 68, 69] $\hat{\Sigma}^r_{L,R}(E)$. They define the level broadening operators, $\hat{\Gamma}_{L,R}(E) = i[\hat{\Sigma}^r_{L,R}(E) - \hat{\Sigma}^a_{L,R}(E)]$, quantifying the electron escape rate into the leads.

The Keldysh formula is valid in the nonlinear regime (i.e., for large V_b) [52, 56, 72]. Thus, to compare it with the Kubo Eq. (1), we assume small $eV_b \ll E_F$, where E_F is the Fermi energy, leading to $f_L - f_R \approx eV_b\,\delta(E-E_F)$ at zero temperature. In such linear-response limit, $\hat{\rho}^{\rm neq}_{\rm Keldysh}$ can be decomposed [52, 73] as (many other decompositions [17] are possible [74, 75])

$$\hat{\rho}^{\rm neq}_{\rm Keldysh} = \hat{\rho}^{\rm surf}_{\rm Keldysh} + \hat{\rho}^{\rm sea}_{\rm Keldysh}, \tag{4a}$$

$$\hat{\rho}^{\rm surf}_{\rm Keldysh} = \frac{eV_b}{2\pi}\hat{G}^r\hat{\Gamma}_L\hat{G}^a, \tag{4b}$$

$$\hat{\rho}^{\rm sea}_{\rm Keldysh} = -\frac{1}{\pi}\int_{-\infty}^{+\infty} dE f_R(E)\,{\rm Im}\,\hat{G}_{V_b}(E) + \frac{1}{\pi}\int_{-\infty}^{\infty} dE f(E)\,{\rm Im}\,\hat{G}(E). \tag{4c}$$

In Eq. (4c) we explicitly subtract the grand canonical density matrix in equilibrium (which is built in into Kubo's derivation [13]), $\hat{\rho}_{\rm eq} = -\frac{1}{\pi}\int_{-\infty}^{\infty} dE f(E)\,{\rm Im}\,\hat{G}(E)$ expressed in terms of GFs, as commonly done [57, 72, 76] to remove expectation values that can be nonzero in equilibrium but are experimentally not observed, such as a

field-like [77, 78] component of spin torque [72, 76], circulating spin currents [57, 79], and circulating charge current [23] (in the presence of external magnetic field).

It may seem at first that the Kubo Eq. (1) and Keldysh Eq. (4) are of quite different form and describing quite different scenarios, that is, bulk transport in the former and two-terminal setups in the latter. Nonetheless, the two formulations are general and should lead to the same physical conclusions. Indeed, their equivalence [17] is well-established [23, 62] for longitudinal charge transport observables requiring only $\hat{\rho}^{\rm surf}_{\rm Kubo}$ or $\hat{\rho}^{\rm surf}_{\rm Keldysh}$. However, notably in the context of spin transport, the use of the two formulations has generated widespread confusion and even highly *divergent conclusions* about the same phenomenon. For example, Ref. [58] compared the spin Hall (SH) current obtained from Keldysh calculations in 4-terminal geometry [57] to that of Kubo calculations on periodic lattices, concluding that the Kubo formula is insufficient. Conversely, in spin-orbit (SO) torque calculations, the Keldysh approach apparently predicts [70, 80] only the field-like (i.e., odd in magnetization [78, 81]) component of SO torque $\mathbf{T}_{\rm Keldysh} \equiv \mathbf{T}^o$ in the clean limit, while Kubo formula yields [82–86] a nonzero value of both $\mathbf{T}^o$ and damping-like (i.e., even in magnetization [78, 81]) SO torque $\mathbf{T}^e$. The even SO torque from the Kubo formula has a well-studied "intrinsic" contribution that is governed [31, 82–84] by the Berry curvature of occupied Fermi-sea states and is largely insensitive to a phenomenological η or even to real-space disorder [30]. Thus, $\mathbf{T}_{\rm Keldysh} \neq \mathbf{T}_{\rm Kubo}$, even when both calculations are performed on an identical system, such as the paradigmatic Rasbha SO- and exchange-coupled two-dimensional (2D) electron gas [80, 83, 84]. This in turn has led to the opposite perception, that is, that the Keldysh formula is insufficient. However, $\eta \to 0$ leads to $\mathbf{T}^o \to \infty$ [Fig. 3(f)] in Kubo calculations of clean systems, which led to concerns [80] about the use of Kubo Eq. (1) in the absence of extrinsic scattering mechanisms. Additionally, calculations via Kubo Eq. (1) with first-principles Hamiltonian $\hat{H}$ of ferromagnet/heavy-metal bilayers, such as Co/Pt, plugged into GF in Eq. (2) *do not* [31, 32] find strongly anisotropic angular features of SO torque, thereby contradicting calculations [78] using Keldysh Eq. (4) with GF in Eq. (2) or experiments [87] on the same Co/Pt system.

In this Letter, we demonstrate the *numerically exact equivalence* between the Kubo and Keldysh approaches by focusing on two paradigmatic examples of coupled spin-charge transport phenomena in spintronics, i.e., the SH effect and the SO torque. We provide a constructive proof of their equivalence by developing numerical frameworks which (*i*) apply the Kubo(-Bastin) density matrix to two-terminal setups [Fig. 1], via Eq. (3) plugged into Eq. (1), which is an unexplored route in studies arriving at *divergent conclusions*; and (*ii*) properly construct [17] $\hat{\rho}^{\rm sea}_{\rm Keldysh}$ contribution to the Keldysh

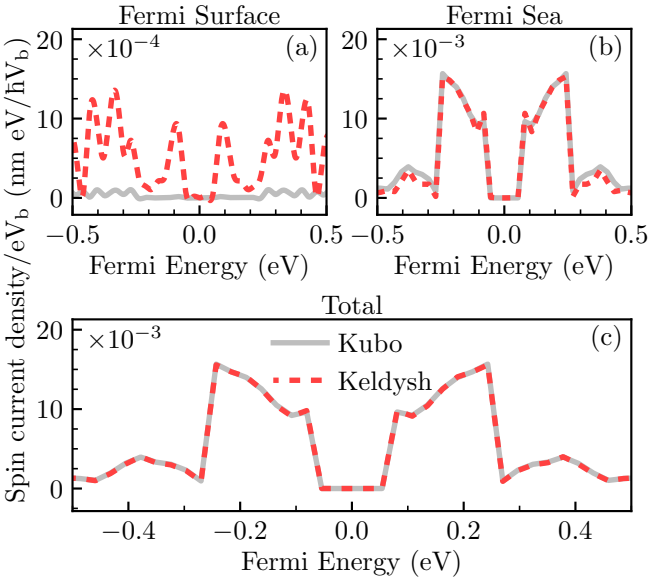

FIG. 2. Spin Hall current density—obtained by tracing its operator [88] with (a) Fermi-surface, (b) Fermi-sea, and (c) total density matrices—in Kubo [Eq. (1)] vs. Keldysh [Eq. (4)] approaches employing the same retarded GF [Eq. (3)] of doubly-proximitized graphene. The parameters in Eq. (5) are set as $\lambda_{\rm RSO} = J_{\rm sd} = 0.1$ eV and the disorder strength is $D = 0.3$ eV. The spin current density is averaged over 200 disorder configurations. Convergence with respect to k_y-point sampling was also established.

density matrix [Eq. (4c)], which requires using (a rarely computed [73, 78]) $\hat{G}^r_{V_b} = \left[E - \hat{H} - eU_i - \hat{\Sigma}^r_L - \hat{\Sigma}^r_R\right]^{-1}$ in Eq. (4c) that includes the voltage drop eU_i across the CA region [Fig. 1]. Note that $\hat{G}^r_{V_b}$ is markedly different from $\hat{G}^r$ [Eq. (3)] used in all other terms of Kubo Eq. (1) or Keldysh Eq. (4). Since a voltage drop *cannot* [63] be justified for clean CA region hosting ballistic charge transport, this also suggests that the computation of local transport quantities always requires the introduction of real-space disorder, even though disorder averaging is often avoided due to the high computational cost of repeated integrations over the Fermi-sea [78] (recently developed spectral algorithms could be used to mitigate this problem [89]). Bulk properties can still be extracted [88] from two-terminal systems with CA region of finite length by computing local quantities at some distance [88, 90] away from the CA-region/lead interface (such as, at the shaded middle hexagons in Fig. 1).

To demonstrate such an equivalence, we compute the SH current [Fig. 2] and SO torque [Fig. 3] densities via Kubo and Keldysh routes for the same system—a graphene sheet with both SO coupling and magnetic ordering [Fig. 1]. The effective TB Hamiltonian (whose parameters can be fitted to first-principles calculations [70]

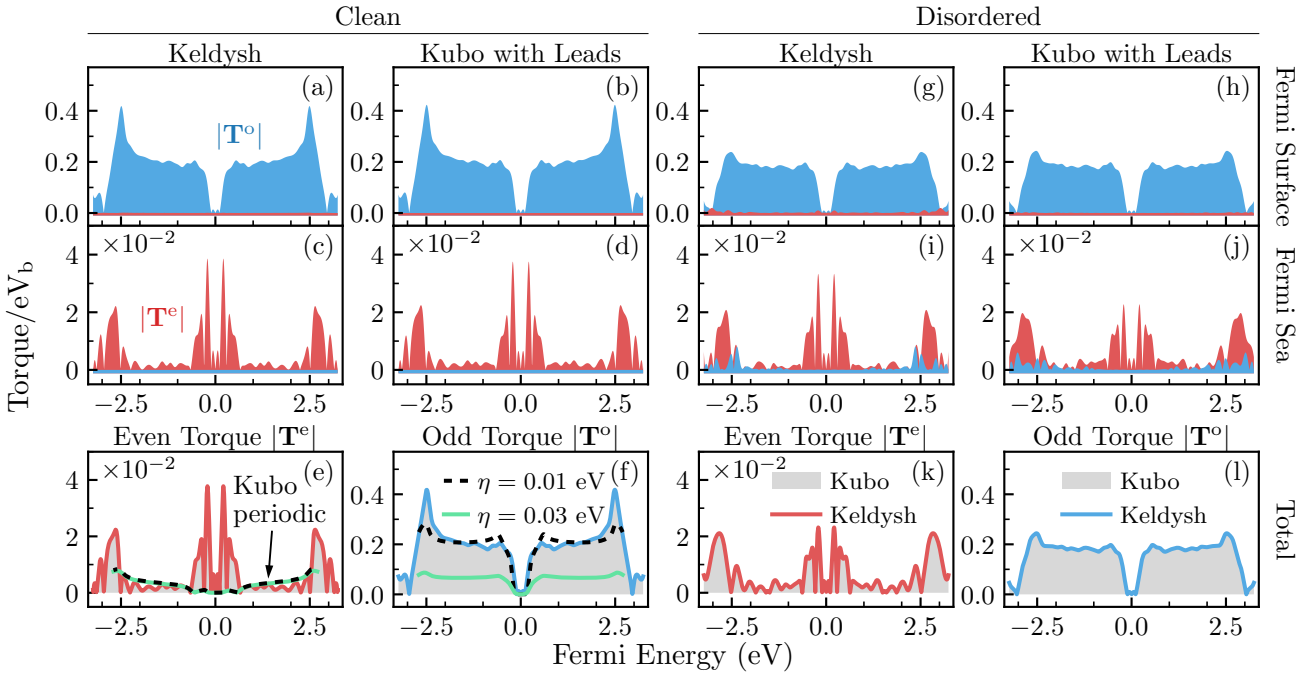

FIG. 3. Similar to Fig. 2, but for even $\mathbf{T}^{e}$ (or damping-like [77, 78]) and odd $\mathbf{T}^{o}$ (or field-like [77, 78]) SO torques. Each row was obtained by tracing the torque operator [75, 78] with (a),(b),(g),(h) Fermi-surface; or (c),(d),(i),(j) Fermi-sea density matrix; as well as (e),(f),(k),(l) total density matrix within Kubo Eq. (1) vs. Keldysh Eq. (4). In panels (a)–(f), the CA region in Fig. 1 is clean, while in panels (g)–(l) it contains Anderson disorder of strength $D = 0.5$ eV. Panels (e) and (f) show additional (black and green) curves obtained from conventional [27, 30–33] Kubo calculations on periodic lattices [i.e., by using Eq. (2) plugged into Eq. (1)]. The parameters in Eq. (5) read as $\lambda_{\rm RSO} = J_{\rm sd} = 0.3$ eV. Calculations with disorder employ 200 configurations.

or experimental data [40]) is given by

$$\hat{H} = -t\sum_{\langle i,j\rangle,\sigma}\hat{c}^{\dagger}_{i\sigma}\hat{c}_{j\sigma} + \frac{2i\lambda_{\rm RSO}}{3}\sum_{\langle i,j\rangle,\sigma\neq\sigma'}[\hat{\boldsymbol{\sigma}}\times\boldsymbol{d}_{ij}]_{\sigma\sigma'}\hat{c}^{\dagger}_{i\sigma}\hat{c}_{j\sigma'} + \sum_{i,\sigma,\sigma'}\hat{c}^{\dagger}_{i\sigma}\Big(\varepsilon_i\delta_{\sigma\sigma'} + J_{\rm sd}[\mathbf{m}_i\cdot\hat{\boldsymbol{\sigma}}]_{\sigma\sigma'}\Big)\hat{c}_{i\sigma'}. \quad (5)$$

Physically, such spin-dependent interactions can be introduced in graphene via proximity effects from an overlayer of 2D ferromagnetic insulator and underlayer of 2D semiconductor material [70]. Here $\hat{c}^{\dagger}_{i\sigma}$ ($\hat{c}_{i\sigma}$) creates (annihilates) an electron at a site i with spin $\sigma =\uparrow,\downarrow$; $\hat{\boldsymbol{\sigma}} = (\hat{\sigma}_x,\hat{\sigma}_y,\hat{\sigma}_z)$ is the vector of the Pauli matrices; $t = 2.7$ eV is the nearest-neighbor (NN) hopping; the sum $\langle i,j\rangle$ goes over all pairs of NN sites; $\varepsilon_i \in [-D/2, D/2]$ is a uniform random variable introducing Anderson disorder on each site; $J_{\rm sd}$ is *sd* exchange coupling between conduction electrons and proximity-induced localized magnetic moments described by a classical unit vector $\mathbf{m}_i$. While other SO effects can be induced in graphene [70, 91], we focus on symmetry-breaking Rashba SO coupling of strength $\lambda_{\rm RSO}$, where $\mathbf{d}_{ij}$ is the unit vector along the direction connecting NN sites i and j. The k-point sampling along the transverse direction is implemented [71] with hoppings connecting sites along the lower and upper edge of armchair nanoribbon multiplied by the phase e^{ik_yW}. All results in Figs. 1(c), 2 and 3 are averaged [71, 92] over the transverse wavevector using $\langle\hat{O}\rangle = \frac{W}{2\pi}\int_{-\pi/W}^{\pi/W}dk_y\,\langle\hat{O}\rangle_{k_y}$. Though not essential for the Kubo vs. Keldysh equivalence, the k-sampling makes the system behave as infinite along the y-axis and thus yields bulk-like [71] behavior [see its density of states in Fig. S1(d) of the SM [17]].

In order to reconcile the Kubo and Keldysh approaches, we start by recalling that for pure Fermi-surface transport properties their equivalence is well-established from long ago [23]. This has been amply confirmed [93] for, e.g., conductance [23, 62, 94] of two-terminal systems [95], including graphene [89, 96] that we also revisit in the SM [17]. Since the conductance formulas [17] for $G_{\rm Kubo} \equiv G_{\rm Keldysh}$ are essentially the expectation value of the *total* current operator [23, 73] in the right lead divided by the voltage drop (i.e., $G = \langle\hat{I}_R\rangle/V_b$, where $\langle\hat{I}_R\rangle = {\rm Tr}\,[\hat{\rho}^{\rm surf}_{\square}\hat{I}_R]$ and $\square$=Kubo or $\square$=Keldysh), this implies equivalence [23] of ${\rm Tr}[\hat{I}_R\hat{\rho}^{\rm surf}_{\rm Kubo}]$ and ${\rm Tr}[\hat{I}_R\hat{\rho}^{\rm surf}_{\rm Keldysh}]$ on the proviso that the retarded GF in Eq. (3) is used. This suggests that the *divergent conclusions* in recent studies of spin-dependent transport stem from attempts to calculate expectation values of *local* quantities that require additional traces of their operators with the *Fermi-sea terms*, $\hat{\rho}^{\rm sea}_{\rm Kubo}$ [Eq. (1c)] or $\hat{\rho}^{\rm sea}_{\rm Keldysh}$ [Eq. (4c)]. To investigate this issue, in Fig. 2 we first consider the expectation value of spin (Hall) current density $\langle\hat{j}^{S_z}_y\rangle$, with the corresponding operator being [88] $\hat{j}^{S_z}_y = \frac{e}{2}(\hat{v}_y\hat{\sigma}_z + \hat{\sigma}_z\hat{v}_y)$. In order to capture

the bulk behavior, this local transport quantity is computed and averaged over a small area in the middle of the CA region as denoted (yellow hexagons) in Fig. 1. Note that $\langle \hat{j}_y^{S_z} \rangle$, or the SH conductivity $\sigma_{\rm SH} = \langle \hat{j}_y^{S_z} \rangle / E_x$, in the pure Rashba model (i.e., with $J_{\rm sd} = 0$) treated by the standard Kubo calculations with periodic boundary conditions has zero contribution from the Fermi-surface due to vertex corrections when both Rashba-split bands are occupied [36, 39]. Interestingly, our calculations for $J_{\rm sd} \neq 0$ [gray curve in Fig. 2] produce a relatively small nonzero value, which we attribute to artifacts of disorder averaging. The suppression of the Fermi-surface contribution to $\hat{j}_y^{S_z}$ in our results is nontrivial since the interplay of Rashba SOC and exchange coupling is expected to generate robust extrinsic SHE via skew scattering, as shown by Boltzmann and Kubo calculations [97] (enhanced intervalley scattering due to the nature of our short-range disorder landscape [97], as well as the non-diffusive nature of our transport simulations, are likely explanations for this behavior). By contrast, the Keldysh calculations [Fig. 2(a),(b)] contain significant contributions from both the Fermi-surface and Fermi-sea. Although this suggests that $\hat{\rho}^{\rm surf}_{\rm Kubo} \neq \hat{\rho}^{\rm surf}_{\rm Keldysh}$ and $\hat{\rho}^{\rm sea}_{\rm Kubo} \neq \hat{\rho}^{\rm sea}_{\rm Keldysh}$, it is the sum of both contributions which carries the physical meaning. Indeed, we see that $\mathrm{Tr}[\hat{\rho}^{\rm neq}_{\rm Keldysh} \hat{j}_y^{S_z}] \equiv \mathrm{Tr}[\hat{\rho}^{\rm neq}_{\rm Kubo} \hat{j}_y^{S_z}]$ perfectly match in Fig. 2(c).

Another local transport quantity that has been a source of *divergent conclusions* is the SO torque [98]—an intensely studied phenomenon over the past decade due to its experimental [82] and technological relevance [99, 100]. In general, spin torques arise [77, 101] due to exchange of spin angular momentum between flowing electrons and localized magnetization. Specifically, injected unpolarized charge current, together with SO coupling, produces nonequilibrium spin density, $\langle \hat{\mathbf{s}}_i \rangle = \mathrm{Tr}\,[\hat{\rho}^{\rm neq}_{\square} \hat{\boldsymbol{\sigma}}]$ where $\hat{\mathbf{s}}_i = \hat{c}^\dagger \hat{\boldsymbol{\sigma}} \hat{c}_i$ is the spin operator, whose computation makes it possible to obtain local SO torque as $\mathbf{T}_i = J_{\rm sd} \langle \hat{\mathbf{s}}_i \rangle \times \mathbf{m}_i$. Both $\square$=Kubo [27, 30–33, 82–85, 102] and $\square$=Keldysh [70, 74, 75, 78, 80, 81, 103] density matrices have been frequently used in SO torque calculations. Similar to Fig. 2, we average local SO torque over the middle of the CA region indicated in Fig. 1 to obtain $\mathbf{T} = \frac{1}{N} \sum_{i=1}^{N} \mathbf{T}_i = \mathbf{T}^e + \mathbf{T}^o$. Figure 3(a)–(f) shows the energy dependence of the even and odd components of $\mathbf{T}$, with magnetization fixed out of plane $\mathbf{M} = \sum_i \mathbf{m}_i \parallel \hat{z}$, calculated for the clean system. Since both formulations in Fig. 3(a)–(f) yield identical $\mathbf{T}^e_{\rm Kubo} \equiv \mathbf{T}^e_{\rm Keldysh}$ and $\mathbf{T}^o_{\rm Kubo} \equiv \mathbf{T}^o_{\rm Keldysh}$, this demonstrates how the Keldysh formula reproduces Fermi-sea-governed even (or damping-like [77, 78]) SO torque $\mathbf{T}^e$ in the clean limit, that was previously considered arising only via the Kubo route [27, 82–84]. In Fig. 3(e),(f), we additionally show the even and odd SO torque produced by conventional usage [27, 30–32] of the Kubo Eq. (1) on periodic lattices. As expected, the particular choice of the *ad hoc* broadening η affects the results for $\mathbf{T}^o$ [Fig. 3(f)], diverging with $\eta \to 0$ which is unphysical [80, 104]. Moreover, $\mathbf{T}^e$ which is independent of η (and, therefore, considered "intrinsic" [82–84]), *deviates* substantially from our Kubo≡Keldysh results for $\mathbf{T}^e$ on two-terminal systems [Fig. 3(e)]. Thus, the implementation of the Kubo(-Bastin) Eq. (1) on two-terminal geometries that we develop here evades ambiguities due to choice of η in finite-size periodic lattice calculations because two-terminal Landauer setups are infinite systems with a *continuous* energy spectrum [51] (as demanded also in the original derivations of Kubo [13, 104–106]) which ensures that dissipation is effectively introduced [107–109]. Our implementation also mimics closely experimental setups where a nonequilibrium state is introduced [23, 104–106] by injecting current through the leads or by applying a voltage difference V_b between them, rather than by applying electric field. In the disordered case, Fig. 3(g) shows that $\hat{\rho}^{\rm surf}_{\rm Keldysh}$ produces additional contributions to damping-like $\mathbf{T}^e$, which we attribute to the often overlooked skew-scattering-induced damping-like SO torque [70, 85, 86, 110]. Also, $\hat{\rho}^{\rm sea}_{\rm Keldysh}$ and $\hat{\rho}^{\rm sea}_{\rm Kubo}$ produce [Fig. 3(i),(j)] additional contributions to $\mathbf{T}^o$. Despite these differences in specific contributions, their sums produce identical $\mathrm{Tr}[\hat{\rho}^{\rm neq}_{\rm Keldysh} \hat{T}_i^{e,o}] \equiv \mathrm{Tr}[\hat{\rho}^{\rm neq}_{\rm Kubo} \hat{T}_i^{e,o}]$ in Fig. 3(k),(l). This, together with the results of Fig. 2(c), completes our proof of equivalence.

The numerical frameworks developed and validated here demonstrate an unambiguous route to study generic spin-charge transport phenomena in the linear-response regime of realistic systems, in addition to resolving a debate in spintronics over the proper usage of Kubo and Keldsyh formulas. Our findings also suggests that assigning a unique and special physical meaning [31, 82–84] to the Fermi-sea term in Kubo [Eq. (1)] requires careful scrutiny, as the decomposition of density matrix into Fermi-surface and Fermi-sea contributions is not unique [17] and, as seen through the demonstrated Kubo vs. Keldysh equivalence, there are many possible [17] (and rather mundane looking) forms of the Fermi-sea term within the Keldysh formalism [Eq. (4)]. The particular expression to be used in practical calculations is a matter of computational convenience [111].

B. K. N. was supported by the US NSF through the University of Delaware Materials Research Science and Engineering Center, DMR-2011824. The supercomputing time was provided by DARWIN (Delaware Advanced Research Workforce and Innovation Network), which is supported by NSF Grant No. MRI-1919839. A. F. acknowledges the partial support from a Royal Society University Research Fellowship.

* aires.ferreira@york.ac.uk

† bnikolic@udel.edu

[1] L. E. Ballentine, *Quantum Mechanics: A Modern Development* (World Scientific, Singapore, 2014).

[2] M. Kardar, *Statistical Physics of Particles* (Cambridge University Press, Cambridge, 2007).

[3] F. Nathan and M. S. Rudner, Quantifying the accuracy of steady states obtained from the universal Lindblad equation, Phys. Rev. B **109**, 205140 (2024).

[4] S. Weinberg, Quantum mechanics without state vectors, Phys. Rev. A **90**, 042102 (2014).

[5] E. Joos, H. D. Zeh, C. Kiefer, D. J. W. Giulini, J. Kupsch, and I. Stamatescu, *Decoherence and the Appearance of a Classical World in Quantum Theory* (Springer-Verlag Berlin, 2003).

[6] F. Garcia-Gaitan and B. K. Nikolić, Fate of entanglement in magnetism under Lindbladian or non-Markovian dynamics and conditions for their transition to Landau-Lifshitz-Gilbert classical dynamics, Phys. Rev. B **109**, L180408 (2024).

[7] P. Dutt, J. Koch, J. E. Han, and K. L. Hur, Effective equilibrium theory of nonequilibrium quantum transport, Ann. Phys. **326**, 2963 (2011).

[8] A. Dhar, K. Saito, and P. Hänggi, Nonequilibrium density-matrix description of steady-state quantum transport, Phys. Rev. E **85**, 011126 (2012).

[9] B. Gaury, J. Weston, M. Santin, M. Houzet, C. Groth, and X. Waintal, Numerical simulations of time-resolved quantum electronics, Phys. Rep. **534**, 1 (2014).

[10] B. S. Popescu and A. Croy, Efficient auxiliary-mode approach for time-dependent nanoelectronics, New J. Phys. **18**, 093044 (2016).

[11] U. Bajpai and B. K. Nikolić, Spintronics meets nonadiabatic molecular dynamics: Geometric spin torque and damping on dynamical classical magnetic texture due to an electronic open quantum system, Phys. Rev. Lett. **125**, 187202 (2020).

[12] M. Ridley, N. W. Talarico, D. Karlsson, N. Lo Gullo, and R. Tuovinen, A many-body approach to transport in quantum systems: from the transient regime to the stationary state, J. Phys. A: Math. Theor. **55**, 273001 (2022).

[13] R. Kubo, Statistical-mechanical theory of irreversible processes. I. general theory and simple applications to magnetic and conduction problems, J. Phys. Soc. Jpn. **12**, 570 (1957).

[14] L. Keldysh, Diagram technique for nonequilibrium processes, Sov. Phys. JETP **20**, 1018 (1965).

[15] G. Stefanucci and R. van Leeuwen, *Nonequilibrium Many-Body Theory of Quantum Systems: A Modern Introduction* (Cambridge University Press, Cambridge, 2013).

[16] A. Bastin, C. Lewiner, O. Betbeder-matibet, and P. Nozieres, Quantum oscillations of the Hall effect of a fermion gas with random impurity scattering, J. Phys. Chem. Solids **32**, 1811 (1971).

[17] See Supplemental Material (SM) at `https://wiki.physics.udel.edu/qttg/Publications`, which includes Ref. [112], for: (i) summary of different commonly employed decompositions of Kubo Eq. (1) and Keldysh Eq. (4), as well as additional details on their numerical evaluation; (ii) one additional figure recalling a well-established [23, 95] equivalence of Kubo and Keldysh formulas for conductance (i.e., longitudinal charge transport) calculations using an example of plain [i.e., without SOC and magnetism terms in Eq. (5)] graphene in Fig. 1; and (iii) for the same plain graphene, we also show that its density of states computed using the setup of Fig. 1 is identical to standard result [113] for infinite graphene.

[18] L. Smrčka and P. Středa, Transport coefficients in strong magnetic fields, J. Phys. C: Solid State Phys. **10**, 2153 (1977).

[19] P. Středa, Theory of quantised Hall conductivity in two dimensions, J. Phys. C: Solid State Phys. **15**, L717 (1982).

[20] A. Crépieux and P. Bruno, Theory of the anomalous Hall effect from the Kubo formula and the Dirac equation, Phys. Rev. B **64**, 014416 (2001).

[21] V. Bonbien and A. Manchon, Symmetrized decomposition of the Kubo-Bastin formula, Phys. Rev. B **102**, 085113 (2020).

[22] I. A. Ado, M. Titov, R. A. Duine, and A. Brataas, Kubo formula for dc conductivity: Generalization to systems with spin-orbit coupling, Phys. Rev. Res. **6**, L012057 (2024).

[23] H. U. Baranger and A. D. Stone, Electrical linear-response theory in an arbitrary magnetic field: A new Fermi-surface formation, Phys. Rev. B **40**, 8169 (1989).

[24] D. A. Greenwood, The Boltzmann equation in the theory of electrical conduction in metals, Prof. Phys. Soc. London **71**, 585 (1958-04).

[25] S. M. João, M. Andjelković, L. Covaci, T. G. Rappoport, J. M. V. P. Lopes, and A. Ferreira, KITE: high-performance accurate modelling of electronic structure and response functions of large molecules, disordered crystals and heterostructures, R. Soc. Open Sci. **7**, 191809 (2020).

[26] Z. Fan, J. H. Garcia, A. W. Cummings, J. E. Barrios-Vargas, M. Panhans, A. Harju, F. Ortmann, and S. Roche, Linear scaling quantum transport methodologies, Phys. Rep. **903**, 1 (2021).

[27] S. Ghosh and A. Manchon, Spin-orbit torque in a three-dimensional topological insulator–ferromagnet heterostructure: Crossover between bulk and surface transport, Phys. Rev. B **97**, 134402 (2018).

[28] D. Van Tuan, J. M. Marmolejo-Tejada, X. Waintal, B. K. Nikolić, S. O. Valenzuela, and S. Roche, Spin Hall effect and origins of nonlocal resistance in adatom-decorated graphene, Phys. Rev. Lett. **117**, 176602 (2016).

[29] J. H. Garcia, A. W. Cummings, and S. Roche, Spin Hall effect and weak antilocalization in graphene/transition metal dichalcogenide heterostructures, Nano Lett. **17**, 5078 (2017).

[30] J. Medina Dueñas, J. H. García, and S. Roche, Emerging spin-orbit torques in low-dimensional Dirac materials, Phys. Rev. Lett. **132**, 266301 (2024).

[31] F. Freimuth, S. Blügel, and Y. Mokrousov, Spin-orbit torques in Co/Pt(111) and Mn/W(001) magnetic bilayers from first principles, Phys. Rev. B **90**, 174423 (2014).

[32] F. Mahfouzi and N. Kioussis, First-principles study of the angular dependence of the spin-orbit torque in Pt/Co and Pd/Co bilayers, Phys. Rev. B **97**, 224426 (2018).

[33] F. Mahfouzi, R. Mishra, P.-H. Chang, H. Yang, and N. Kioussis, Microscopic origin of spin-orbit torque in ferromagnetic heterostructures: A first-principles approach, Phys. Rev. B **101**, 060405 (2020).

[34] F. J. d. Santos, D. A. Bahamon, R. B. Muniz, K. McKenna, E. V. Castro, J. Lischner, and A. Ferreira, Impact of complex adatom-induced interactions on quantum spin Hall phases, Phys. Rev. B **98**, 081407 (2018).

[35] E. N. Economou, *Green's Functions in Quantum Physics* (Springer, Berlin, 2006).

[36] O. V. Dimitrova, Spin-Hall conductivity in a two-dimensional Rashba electron gas, Phys. Rev. B **71**, 245327 (2005).

[37] I. A. Ado, I. A. Dmitriev, P. M. Ostrovsky, and M. Titov, Anomalous Hall effect with massive Dirac fermions, Europhysics Letters **111**, 37004 (2015).

[38] M. Milletarì and A. Ferreira, Quantum diagrammatic theory of the extrinsic spin Hall effect in graphene, Phys. Rev. B **94**, 134202 (2016).

[39] M. Milletarì, M. Offidani, A. Ferreira, and R. Raimondi, Covariant conservation laws and the spin Hall effect in Dirac-Rashba systems, Phys. Rev. Lett. **119**, 246801 (2017).

[40] D. T. S. Perkins, A. Veneri, and A. Ferreira, Spin Hall effect: Symmetry breaking, twisting, and giant disorder renormalization, Phys. Rev. B **109**, L241404 (2024).

[41] Y. Imry, *Introduction to Mesoscopic Physics* (Oxford University Press, Oxford, 2002).

[42] K. Nomura and A. H. MacDonald, Quantum transport of massless Dirac fermions, Phys. Rev. Lett. **98**, 076602 (2007).

[43] J. P. Santos Pires, S. M. João, A. Ferreira, B. Amorim, and J. M. Viana Parente Lopes, Anomalous transport signatures in Weyl semimetals with point defects, Phys. Rev. Lett. **129**, 196601 (2022).

[44] D. J. Thouless and S. Kirkpatrick, Conductivity of the disordered linear chain, J. Phys. C: Solid State Phys. **14**, 235 (1981).

[45] S. M. João, J. M. Viana Parente Lopes, and A. Ferreira, High-resolution real-space evaluation of the self-energy operator of disordered lattices: Gade singularity, spin–orbit effects and p-wave superconductivity, J. Phys. Mater. **5**, 045002 (2022).

[46] J. P. Boyd, *Chebyshev and Fourier Spectral Methods* (DOVER Publications, New York, 2000).

[47] A. Weiße, G. Wellein, A. Alvermann, and H. Fehske, The kernel polynomial method, Rev. Mod. Phys. **78**, 275 (2006).

[48] A. Ferreira and E. R. Mucciolo, Critical delocalization of chiral zero energy modes in graphene, Phys. Rev. Lett. **115**, 106601 (2015).

[49] F. M. O. Brito and A. Ferreira, Real-space spectral simulation of quantum spin models: Application to generalized Kitaev models, SciPost Phys. Core **7**, 006 (2024).

[50] P. Bulanchuk, On the delta function broadening in the Kubo-Greenwood equation, Comp. Phys. Commun. **261**, 107714 (2021).

[51] X. Waintal, M. Wimmer, A. Akhmerov, C. Groth, B. K. Nikolić, M. Istas, T. Örn Rosdahl, and D. Varjas, Computational quantum transport, arXiv:2407.16257 (2024).

[52] M. Brandbyge, J.-L. Mozos, P. Ordejón, J. Taylor, and K. Stokbro, Density-functional method for nonequilibrium electron transport, Phys. Rev. B **65**, 165401 (2002).

[53] B. K. Nikolić, S. Souma, L. P. Zârbo, and J. Sinova, Nonequilibrium spin Hall accumulation in ballistic semiconductor nanostructures, Phys. Rev. Lett. **95**, 046601 (2005).

[54] A. Reynoso, G. Usaj, and C. A. Balseiro, Spin Hall effect in clean two-dimensional electron gases with Rashba spin-orbit coupling, Phys. Rev. B **73**, 115342 (2006).

[55] P. M. Haney, D. Waldron, R. A. Duine, A. S. Núñez, H. Guo, and A. H. MacDonald, Current-induced order parameter dynamics: Microscopic theory applied to co/cu/co spin valves, Phys. Rev. B **76**, 024404 (2007).

[56] D. A. Areshkin and B. K. Nikolić, I-V curve signatures of nonequilibrium-driven band gap collapse in magnetically ordered zigzag graphene nanoribbon two-terminal devices, Phys. Rev. B **79**, 205430 (2009).

[57] B. K. Nikolić, L. P. Zârbo, and S. Souma, Imaging mesoscopic spin Hall flow: Spatial distribution of local spin currents and spin densities in and out of multiterminal spin-orbit coupled semiconductor nanostructures, Phys. Rev. B **73**, 075303 (2006).

[58] S. A. Gulbrandsen, C. Espedal, and A. Brataas, Spin Hall effect in antiferromagnets, Phys. Rev. B **101**, 184411 (2020).

[59] Y. Imry and R. Landauer, Conductance viewed as transmission, Rev. Mod. Phys. **71**, S306 (1999).

[60] Y. V. Nazarov and Y. M. Blanter, *Quantum Transport: Introduction to Nanoscience* (Cambridge University Press, Cambridge, 2009).

[61] C. Caroli, R. Combescot, P. Nozieres, and D. Saint-James, Direct calculation of the tunneling current, J. Phys. C: Solid State Phys. **4**, 916 (1971).

[62] D. S. Fisher and P. A. Lee, Relation between conductivity and transmission matrix, Phys. Rev. B **23**, 6851 (1981).

[63] M. C. Payne, Electrostatic and electrochemical potentials in quantum transport, J. Phys.: Condens. Matter **1**, 4931 (1989).

[64] Y. Meir and N. S. Wingreen, Landauer formula for the current through an interacting electron region, Phys. Rev. Lett. **68**, 2512 (1992).

[65] H. Ness, L. K. Dash, and R. W. Godby, Generalization and applicability of the Landauer formula for nonequilibrium current in the presence of interactions, Phys. Rev. B **82**, 085426 (2010).

[66] F. Mahfouzi and B. K. Nikolić, Signatures of electron-magnon interaction in charge and spin currents through magnetic tunnel junctions: A nonequilibrium many-body perturbation theory approach, Phys. Rev. B **90**, 045115 (2014).

[67] H. Ness and L. K. Dash, Nonequilibrium quantum transport in fully interacting single-molecule junctions, Phys. Rev. B **84**, 235428 (2011).

[68] J. Velev and W. Butler, On the equivalence of different techniques for evaluating the green function for a semi-infinite system using a localized basis, J. Phys.: Condens. Matter **16**, R637 (2004).

[69] I. Rungger and S. Sanvito, Algorithm for the construction of self-energies for electronic transport calculations based on singularity elimination and singular value decomposition, Phys. Rev. B **78**, 035407 (2008).

[70] K. Zollner, M. D. Petrović, K. Dolui, P. Plecháč, B. K. Nikolić, and J. Fabian, Scattering-induced and highly tunable by gate damping-like spin-orbit torque in graphene doubly proximitized by two-dimensional magnet $Cr_2Ge_2Te_6$ and monolayer WS_2, Phys. Rev. Res. **2**,

043057 (2020).
[71] M.-H. Liu and K. Richter, Efficient quantum transport simulation for bulk graphene heterojunctions, Phys. Rev. B **86**, 115455 (2012).
[72] M. O. A. Ellis, M. Stamenova, and S. Sanvito, Multiscale modeling of current-induced switching in magnetic tunnel junctions using *ab initio* spin-transfer torques, Phys. Rev. B **96**, 224410 (2017).
[73] F. Mahfouzi and B. K. Nikolić, How to construct the proper gauge-invariant density matrix in steady-state nonequilibrium: Applications to spin-transfer and spin-orbit torques, SPIN **3**, 1330002 (2013).
[74] F. Mahfouzi, B. K. Nikolić, and N. Kioussis, Antidamping spin-orbit torque driven by spin-flip reflection mechanism on the surface of a topological insulator: A time-dependent nonequilibrium green function approach, Phys. Rev. B **93**, 115419 (2016).
[75] B. K. Nikolić, K. Dolui, M. Petrović, P. Plecháč, T. Markussen, and K. Stokbro, First-principles quantum transport modeling of spin-transfer and spin-orbit torques in magnetic multilayers, in *Handbook of Materials Modeling*, edited by W. Andreoni (Springer, Cham, 2018) pp. 1–35, arXiv:1801.05793.
[76] I. Theodonis, N. Kioussis, A. Kalitsov, M. Chshiev, and W. H. Butler, Anomalous bias dependence of spin torque in magnetic tunnel junctions, Phys. Rev. Lett. **97**, 237205 (2006).
[77] D. Ralph and M. Stiles, Spin transfer torques, J. Magn. Magn. Mater. **320**, 1190 (2008).
[78] K. D. Belashchenko, A. A. Kovalev, and M. van Schilfgaarde, First-principles calculation of spin-orbit torque in a Co/Pt bilayer, Phys. Rev. Materials **3**, 011401 (2019).
[79] E. I. Rashba, Spin currents in thermodynamic equilibrium: The challenge of discerning transport currents, Phys. Rev. B **68**, 241315 (2003).
[80] A. Kalitsov, S. A. Nikolaev, J. Velev, M. Chshiev, and O. Mryasov, Intrinsic spin-orbit torque in a single-domain nanomagnet, Phys. Rev. B **96**, 214430 (2017).
[81] K. Dolui, M. D. Petrović, K. Zollner, P. Plecháč, J. Fabian, and B. K. Nikolić, Proximity spin-orbit torque on a two-dimensional magnet within van der waals heterostructure: Current-driven antiferromagnet-to-ferromagnet reversible nonequilibrium phase transition in bilayer CrI_3, Nano Lett. **20**, 2288 (2020).
[82] H. Kurebayashi, J. S. D. Fang, A. C. Irvine, T. D. Skinner, J. Wunderlich, V. Novák, R. P. Campion, B. L. Gallagher, E. K. Vehstedt, L. P. Zârbo, K. Výborný, A. J. Ferguson, and T. Jungwirth, An antidamping spin-orbit torque originating from the berry curvature, Nat. Nanotech. **9**, 211 (2014).
[83] K.-S. Lee, D. Go, A. Manchon, P. M. Haney, M. D. Stiles, H.-W. Lee, and K.-J. Lee, Angular dependence of spin-orbit spin-transfer torques, Phys. Rev. B **91**, 144401 (2015).
[84] H. Li, H. Gao, L. P. Zârbo, K. Výborný, X. Wang, I. Garate, F. Doğan, A. Čejchan, J. Sinova, T. Jungwirth, and A. Manchon, Intraband and interband spin-orbit torques in noncentrosymmetric ferromagnets, Phys. Rev. B **91**, 134402 (2015).
[85] F. Sousa, G. Tatara, and A. Ferreira, Skew-scattering-induced giant antidamping spin-orbit torques: Collinear and out-of-plane edelstein effects at two-dimensional material/ferromagnet interfaces, Phys. Rev. Res. **2**, 043401 (2020).
[86] A. Veneri, D. T. S. Perkins, and A. Ferreira, Nonperturbative approach to interfacial spin-orbit torques induced by the Rashba effect, Phys. Rev. B **106**, 235419 (2022).
[87] K. Garello, I. M. Miron, C. O. Avci, F. Freimuth, Y. Mokrousov, S. Blügel, S. Auffret, O. Boulle, G. Gaudin, and P. Gambardella, Symmetry and magnitude of spin–orbit torques in ferromagnetic heterostructures, Nat. Nanotech. **8**, 587 (2013).
[88] L. Wang, R. J. H. Wesselink, Y. Liu, Z. Yuan, K. Xia, and P. J. Kelly, Giant room temperature interface spin hall and inverse spin Hall effects, Phys. Rev. Lett. **116**, 196602 (2016).
[89] S. G. de Castro, J. a. M. V. P. Lopes, A. Ferreira, and D. A. Bahamon, Fast Fourier-Chebyshev approach to real-space simulations of the Kubo formula, Phys. Rev. Lett. **132**, 076302 (2024).
[90] K. D. Belashchenko, G. G. Baez Flores, W. Fang, A. A. Kovalev, M. van Schilfgaarde, P. M. Haney, and M. D. Stiles, Breakdown of the drift-diffusion model for transverse spin transport in a disordered pt film, Phys. Rev. B **108**, 144433 (2023).
[91] D. Perkins and A. Ferreira, Spintronics in 2D graphene-based van der Waals heterostructures, in *Encyclopedia of Condensed Matter Physics*, edited by T. Chakraborty (Academic Press, Oxford, 2024) pp. 205–222.
[92] K. S. Thygesen and K. W. Jacobsen, Interference and k-point sampling in the supercell approach to phase-coherent transport, Phys. Rev. B **72**, 033401 (2005).
[93] Nevertheless, confusion occasionally arises in the literature, such as in Fig. 6 of Ref. [26] where the Kubo conductivity incorrectly does not match quantized conductance from Keldysh approach.
[94] C. L. Kane, R. A. Serota, and P. A. Lee, Long-range correlations in disordered metals, Phys. Rev. B **37**, 6701 (1988).
[95] B. K. Nikolić, Deconstructing Kubo formula usage: Exact conductance of a mesoscopic system from weak to strong disorder limit, Phys. Rev. B **64**, 165303 (2001).
[96] S. G. de Castro, A. Ferreira, and D. A. Bahamon, Efficient Chebyshev polynomial approach to quantum conductance calculations: Application to twisted bilayer graphene, Phys. Rev. B **107**, 045418 (2023).
[97] M. Offidani and A. Ferreira, Anomalous Hall effect in 2D Dirac materials, Phys. Rev. Lett. **121**, 126802 (2018).
[98] A. Manchon, J. Železný, I. M. Miron, T. Jungwirth, J. Sinova, A. Thiaville, K. Garello, and P. Gambardella, Current-induced spin-orbit torques in ferromagnetic and antiferromagnetic systems, Rev. Mod. Phys. **91**, 035004 (2019).
[99] N. Locatelli, V. Cros, and J. Grollier, Spin-torque building blocks, Nat. Mater. **13**, 11 (2014).
[100] W. A. Borders, H. Akima, S. Fukami, S. Moriya, S. Kurihara, Y. Horio, S. Sato, and H. Ohno, Analogue spin-orbit torque device for artificial-neural-network-based associative memory operation, Appl. Phys. Expr. **10**, 013007 (2017).
[101] M. D. Petrović, P. Mondal, A. E. Feiguin, P. Plecháč, and B. K. Nikolić, Spintronics meets density matrix renormalization group: Quantum spin-torque-driven nonclassical magnetization reversal and dynamical buildup of long-range entanglement, Phys. Rev. X **11**, 021062 (2021).
[102] I. A. Ado, O. A. Tretiakov, and M. Titov, Microscopic

theory of spin-orbit torques in two dimensions, Phys. Rev. B **95**, 094401 (2017).
[103] K. D. Belashchenko, A. A. Kovalev, and M. van Schilfgaarde, Interfacial contributions to spin-orbit torque and magnetoresistance in ferromagnet/heavy-metal bilayers, Phys. Rev. B **101**, 020407 (2020).
[104] J. Wu and M. Berciu, Kubo formula for open finite-size systems, EPL (Europhysics Letters) **92**, 30003 (2010).
[105] A. Kundu, A. Dhar, and O. Narayan, The Green–Kubo formula for heat conduction in open systems, J. Stat. Mech. Theor. Exp. **2009**, L03001 (2009).
[106] N. Kamiya and S. Takesue, Kubo formula for finite open quantum systems, J. Phys. Soc. Jpn. **82**, 114002 (2013).
[107] G. Giuliani and G. Vignale, *Quantum Theory of the Electron Liquid* (Cambridge University Press, Cambridge, 2008).
[108] M. D. Petrović, B. S. Popescu, U. Bajpai, P. Plecháč, and B. K. Nikolić, Spin and charge pumping by a steady or pulse-current-driven magnetic domain wall: A self-consistent multiscale time-dependent quantum-classical hybrid approach, Phys. Rev. Applied **10**, 054038 (2018).
[109] J. Varela-Manjarres and B. K. Nikolić, High-harmonic generation in spin and charge current pumping at ferromagnetic or antiferromagnetic resonance in the presence of spin-orbit coupling, J. Phys. Mater. **6**, 045001 (2023).
[110] J. Y. Zhang, P. W. Dou, R. Y. Liu, Y. B. Wang, X. Deng, L. Y. Feng, X. Q. Zheng, H. Huang, and S. G. Wang, Enhanced spin orbit torque efficiency induced by large skew scattering in perpendicular Pt/Co/Ta multilayers with superlattice/alloying Nb (Ir) insertion, Appl. Phys. Lett. **123**, 182401 (2023).
[111] Note that in the "symmetrized decomposition" of Ref. [21], the integrand in Eq. (1c) is not analytic in the upper complex plane, which introduces additional computational complexity. In some other decompositions, and for the integration in Eq. (4c), many efficient complex contour-based algorithms have been developed [52, 114, 115], see the SM for more details.
[112] S. Mousavi, J. Pask, and N. Sukumar, Efficient adaptive integration of functions with sharp gradients and cusps in n-dimensional parallelepipeds, Int. J. Numer. Methods Eng. **91**, 343 (2012).
[113] A. H. Castro Neto, F. Guinea, N. M. R. Peres, K. S. Novoselov, and A. K. Geim, The electronic properties of graphene, Rev. Mod. Phys. **81**, 109 (2009).
[114] T. Ozaki, Continued fraction representation of the Fermi-Dirac function for large-scale electronic structure calculations, Phys. Rev. B **75**, 035123 (2007).
[115] D. A. Areshkin and B. K. Nikolić, Electron density and transport in top-gated graphene nanoribbon devices: First-principles green function algorithms for systems containing a large number of atoms, Phys. Rev. B **81**, 155450 (2010).

Supplemental Material for "Reconciling Kubo and Keldysh Approaches to Fermi-sea-dependent Nonequilibrium Observables: Application to Spin Hall Effect and Spin-Orbit Torque in Spintronics"

Simão M. João,[1] Marko D. Petrović,[2] J. M. Viana Parente Lopes,[3] Aires Ferreira,[4,*] and Branislav K. Nikolić[2,†]

[1] *Department of Materials, Imperial College London, London SW7 2AZ, UK*
[2] *Department of Physics and Astronomy, University of Delaware, Newark, DE 19716, USA*
[3] *Centro de Física das Universidades do Minho e Porto and Departamento de Física e Astronomia, Faculdade de Ciências, Universidade do Porto, 4169-007 Porto, Portugal*
[4] *Department of Physics, University of York, YO10 5DD, York, UK*

This Supplemental Material provides: (i) summary of different commonly employed decompositions of Kubo and Keldysh formulas used in the main text, as well as additional details on their numerical evaluation; (ii) one additional Fig. S1(a)–(c) recalling a well-established [1, 2] equivalence of Kubo and Keldysh formulas for conductance (i.e., longitudinal charge transport) calculations using an example of plain [i.e., without SOC and magnetism terms in Eq. (5) of the main text] graphene in Fig. 1 of the main text; and (iii) for the same plain graphene, we also show in Fig. S1(d) that its density of states (DOS) computed using the two-terminal setup of Fig. 1 in the main text is identical to standard result [3] for infinite graphene. We remind the reader that our two-terminal setup in Fig. 1 of the main text uses a longitudinal electric field $\mathbf{E} = E_x \mathbf{e}_x$ applied within the central active (CA) region of length L, such that the leads have bias voltage $V_b = E_x L$ applied between them with electric potential dropping linearly within CA region.

I. DIFFERENT DECOMPOSITIONS OF KUBO(-BASTIN) EQ. (1) IN THE MAIN TEXT

The nonequilibrium expectation value of an operator $\hat{O}$ of a noninteracting electron system brought out of equilibrium due to an applied DC electric field of strength E_x in the linear-response regime is given by

$$\left\langle \hat{O} \right\rangle = \frac{\hbar}{2\pi} e E_x \int_{-\infty}^{\infty} dE f(E) \, \mathrm{Tr} \left[\left(\hat{O} \frac{d\hat{G}^r}{dE} \hat{v}_x - \hat{v}_x \frac{dG^r}{dE} \hat{O} \right) \left(\hat{G}^r - G^a \right) \right], \tag{1}$$

in the Kubo-Bastin formulation [4]. Here $f(E)$ is the Fermi distribution function, $\hat{v}_x$ is the component of the velocity operator along the same direction as the applied electric field and G^r (G^a) is the retarded (advanced) Green's function (GF) which are functions of energy. The trace is over the Hilbert space of states within CA region, while semi-infinite leads are incorporated via self-energies within GF [as shown in Eq. (3) of the main text]. The integration over energy is cumbersome [5] to handle numerically directly on the real energy axis due to sharp peaks [6] of GF, so one usually decomposes Eq. (1) into terms amenable to efficient computation while also attaching a sound physical interpretation to them [7].

A. Smrčka-Středa decomposition

The so-called Smrčka-Středa formula [8, 9] decomposes the Kubo-Bastin Eq. (1) into a term which is localized around the Fermi energy $\langle \hat{O} \rangle_{\mathrm{I}}$ and, therefore, does not require numerical effort; and a term which samples the entire Fermi sea $\langle \hat{O} \rangle_{\mathrm{II}}$, namely

$$\langle \hat{O} \rangle_{\mathrm{I}} = \frac{\hbar}{2\pi} e E_x \int dE \frac{df}{dE} \mathrm{Re}\mathrm{Tr} \left[\hat{O} \hat{G}^r \hat{v}_x \left(\hat{G}^r - \hat{G}^a \right) \right], \tag{2a}$$

$$\langle \hat{O} \rangle_{\mathrm{II}} = \frac{\hbar}{2\pi} e E_x \int dE f(E) \, \mathrm{Re}\mathrm{Tr} \left[\hat{O} \hat{G}^r \hat{v}_x \frac{d\hat{G}^r}{dE} - \hat{O} \frac{d\hat{G}^r}{dE} \hat{v}_x \hat{G}^r \right]. \tag{2b}$$

Since $\langle A \rangle_{\mathrm{II}}$ is analytic in the upper complex plane, it can be computed efficiently using Ozaki contour integration [10] with that plane. Typically, only a couple of hundred poles are required to satisfactorily converge this quantity. The energy derivative of GF in Eq. (2b) is computed numerically using finite difference.

* aires.ferreira@york.ac.uk
† bnikolic@udel.edu

B. Symmetrized decomposition of Bonbien and Manchon

The symmetrized decomposition introduced recently in Ref. [11] redefines Fermi surface and sea terms in Eq. (2) to ensure no overlap between them. Its surface term then becomes identical to the familiar Kubo-Greenwood (KG) formula [1, 12] for longitudinal charge transport properties, and the sea term contains the remaining contributions so that $\langle\hat{O}\rangle_{\rm KG}+\langle\hat{O}\rangle_{\rm sea}\equiv\langle\hat{O}\rangle_{\rm I}+\langle\hat{O}\rangle_{\rm II}$, where

$$\langle\hat{O}\rangle_{\rm KG}=\frac{\hbar}{4\pi}eE_x\int dE\frac{df}{dE}{\rm ReTr}\left[\hat{O}\left(\hat{G}^r-\hat{G}^a\right)\hat{v}_x\left(\hat{G}^r-\hat{G}^a\right)\right], \tag{3a}$$

$$\langle\hat{O}\rangle_{\rm sea}=\frac{\hbar}{2\pi}eE_x\int dE f\left(E\right){\rm ReTr}\left[\hat{O}\left(\hat{G}^r-\hat{G}^a\right)\hat{v}_x\left(\frac{d\hat{G}^r}{dE}+\frac{d\hat{G}^a}{dE}\right)\right]. \tag{3b}$$

An additional overlap term can be defined as

$$\langle\hat{O}\rangle_{\rm ov}=\frac{\hbar}{4\pi}eE_x\int dE\frac{df}{dE}{\rm ReTr}\left[\hat{O}\hat{G}^a\hat{v}_x\hat{G}^r-\hat{O}\hat{G}^r\hat{v}_x\hat{G}^a\right], \tag{4}$$

which facilitates the comparison between the symmetrized decomposition and the Smrčka-Středa decomposition of Sec. I A. That is,

$$\langle\hat{O}\rangle_{\rm sea}=\langle\hat{O}\rangle_{\rm II}+\langle\hat{O}\rangle_{\rm ov}, \tag{5}$$

$$\langle\hat{O}\rangle_{\rm KG}=\langle\hat{O}\rangle_{\rm I}-\langle\hat{O}\rangle_{\rm ov}. \tag{6}$$

Many other decompositions are obviously possible.

In the main text, we used the symmetrized decomposition for comparison with Keldysh formula because of close connection between $\langle\hat{O}\rangle_{\rm KG}$ and surface term in Keldysh formula, see Sec. IV. However, because functions $\hat{G}^r(E)$ and $\hat{G}^a(E)$ nonanalytic below and above the real axis, respectively, their product is nonanalytic function in the entire complex energy plane, thereby rendering Eq. (3b) nonnalytic and not amenable to contour integration techniques. Its direct integration over the real axis can introduce numerical artifacts [5, 6] which make it impossible to achieve exact numerical equivalence with Keldysh formula. Therefore, in practical calculations we obtain $\langle\hat{O}\rangle_{\rm sea}$ from Eq. (5), which means that we first compute $\langle\hat{O}\rangle_{\rm II}$ [Eq. (2b)] from Smrčka-Středa decomposition of Sec. I A via Ozaki contour integration, and then we simply add the overlap term $\langle\hat{O}\rangle_{\rm ov}$ [Eq. (4)], which does not require any integration at zero temperature, onto it.

II. DIFFERENT DECOMPOSITIONS OF KELDYSH EQ. (4) IN THE MAIN TEXT

In the Keldysh GF formalism [13], the nonequilibrium expectation value of the observable $\hat{O}$ in steady-state is given by

$$\langle\hat{O}\rangle=\int dE{\rm Tr}\left[\hat{O}\hat{G}^<\right], \tag{7}$$

where $\hat{G}^<(E)$ is the lesser GF [13] in steady-state nonequilibrium (discussed further in the main text for the case of noninteracting electrons). Equation (7) can also be separated [5] into a Fermi surface and a Fermi sea contributions

$$\langle\hat{O}\rangle_{\rm surf}=\frac{i}{2\hbar}\int dE\big[f_L(E)-f_R(E)\big]{\rm Tr}\left[\hat{O}\hat{G}^r_{V_b}\left(\hat{\Gamma}_L-\hat{\Gamma}_R\right)\hat{G}^a_{V_b}\right], \tag{8a}$$

$$\langle\hat{O}\rangle_{\rm sea}=-\int dE\big[f_R(E)+f_L(E)\big]{\rm ImTr}\left[\hat{O}\hat{G}^r_{V_b}\right], \tag{8b}$$

where $f_L(E)$ [$f_R(E)$] is the Fermi distribution function of the left (L) [right (R)] macroscopic reservoir into which semi-infinite leads terminate and $\hat{\Gamma}_L$ ($\hat{\Gamma}_R$) are the level broadening functions due to semi-infinite leads. The retarded GF $G^r_{V_b}$ introduced in the main text contains local and linear potential drop eU_i along the sample, which must be included along the diagonal of CA region Hamiltonian.

To compare Keldysh Eq. (8) with the Kubo-Bastin formula decompositions of Sec. I requires a linearized version of Keldysh Eq. (8). Recognizing that f_L-f_R is only nonzero in an energy window of size eV_b (at zero temperature, or

slightly longer at nonzero temperature), for small V_b of the linear-response regime the surface term $\langle \hat{O}A \rangle_{\rm surf}$ to first order in V_b becomes simply

$$\langle \hat{O} \rangle_{\rm surf,lin} = \frac{i}{2\hbar} V_b {\rm Tr}\left[\hat{O} G^r \left(\hat{\Gamma}_L - \hat{\Gamma}_R \right) \hat{G}^a \right], \tag{9}$$

where all quantities $\hat{G}^r(E)$, $\hat{G}^a(E)$, $\hat{\Gamma}_L(E)$ and $\hat{\Gamma}_R(E)$ are evaluated at the Fermi energy $E = E_F$ at zero temperature. Since this term is already linear in V_b, any additional V_b contribution coming from the GF $\hat{G}_{V_b}$ is a higher order effect, so that one uses $\hat{G}^r$ in Eq. (9) instead of $\hat{G}^r_{V_b}$. In contrast, the Fermi sea term $\langle \hat{O} \rangle_{\rm sea}$ contains a zeroth and first order term coming from $f_R + f_L$ and another zeroth and first order term coming from $G^r_{V_b}$. Clearly, the existence of zeroth order terms on both factors implies that the potential drop in the GF cannot be disregarded. Thus, we obtain $\langle \hat{O} \rangle_{\rm sea,lin}$ as follows

$$\langle \hat{O} \rangle_{\rm sea,lin} = -\int dE \big[f_R(E) + f_L(E) \big] {\rm Im Tr}\left[\hat{O} \hat{G}^r_{V_b} \right] + 2 \int dE f\left(E\right) {\rm Im Tr}\left[\hat{O} \hat{G}^r \right], \tag{10}$$

where we compute the first term for a very small value of V_b. Given that $\hat{G}^r$ is an analytic function in the upper complex plane, each of the two integrals can be evaluated numerically using contour integration along the Ozaki contour [10] within that plane.

III. CONSIDERATIONS ON NUMERICAL CONVERGENCE

We carried out a careful convergence analysis. The Fermi sea integrals–such as Keldysh sea term [Eq. (10)] or Kubo-Smrčka-Středa II term [Eq. (2b)]—were tested for convergence with respect to temperature and number of poles used for in Ozaki contour integration. The numerical derivatives $d\hat{G}^{r,a}/dE$ were tested for convergence with respect to finite difference parameter h in $d\hat{G}^{r,a}/dE \mapsto \left[\hat{G}^{r,a}(E+h) - \hat{G}^{r,a}(E) \right]/h$. The small but finite value of bias voltage V_b in $\langle \hat{O} \rangle_{\rm sea,lin}$ [Eq. (10)] was also carefully tested to ensure linearity. Finally, expectation values of observables were averaged simultaneously over disorder configurations (when applicable) and k_y points for periodically repeated two-terminal setup along the transverse y-direction in Fig. 1 of the main text, each of these being subject to the convergence analysis.

IV. TWO-TERMINAL CONDUCTANCE: A FAMILIAR EXAMPLE OF KUBO VS. KELDYSH EQUIVALENCE

In this Section, we use example of plain [i.e., without SOC and magnetism terms in Eq. (5) of the main text] infinite graphene to recall well-established [1, 2] equivalence of Kubo and Keldysh formulas, $G_{\rm Kubo} \equiv G_{\rm Keldysh} = \lim_{V_b \to 0} I/V_b$, for longitudinal charge transport quantities that depend only on Fermi surface states. Here I is (absolute value) of charge current flowing through either lead of a two-terminal system. To show that the two formalisms yield the same conductance, one must deploy them on an identical geometry and, therefore, employ the same GF in both calculations, such as retarded GF from Eq. (3) in the main text when using two-terminal setup in Fig. 1 of the main text. Figure S1 demonstrates that

$$G_{\rm Kubo} = \frac{4e^2}{h} \frac{1}{L^2} {\rm Tr}\left(\hat{v}_{\rm x} \, {\rm Im}\hat{G} \, \hat{v}_{\rm x} \, {\rm Im}\hat{G} \right), \tag{11}$$

and Keldysh

$$G_{\rm Keldysh} = \frac{2e^2}{h} {\rm Tr}\left(\hat{\Gamma}_{\rm R} \hat{G}^r \hat{\Gamma}_{\rm L} \hat{G}^a \right), \tag{12}$$

conductances are identical, such as: for single k_y point (for which they are also quantized [2]) in Fig. S1(a); after averaging of many k_y-points in Fig. S1(b); as well as after averaging over both k_y points and disorder introduced as vacancies into honeycomb lattice of graphene, see Fig. S1(c). Since conductance formulas in Eqs. (11) and (12) can be viewed as the trace of Fermi surface contributions to nonequilbrium density matrices $\hat{\rho}^{\rm surf}_{\rm Kubo}$ [Eq. (1b) in the main text] or $\hat{\rho}^{\rm surf}_{\rm Keldysh}$ [Eq. (4b) in the main text] with the operator of total charge current [1] in the right lead $\hat{I}_R$, respectively, this implies equivalence of these density matrices. It also shows [Figs. S1(a) and S1(b)] that $G_{\rm Kubo}$ can be applied even to ballistic transport through a clean system, for which it reproduces [14] conductance quantization [15–17] in mesoscopic

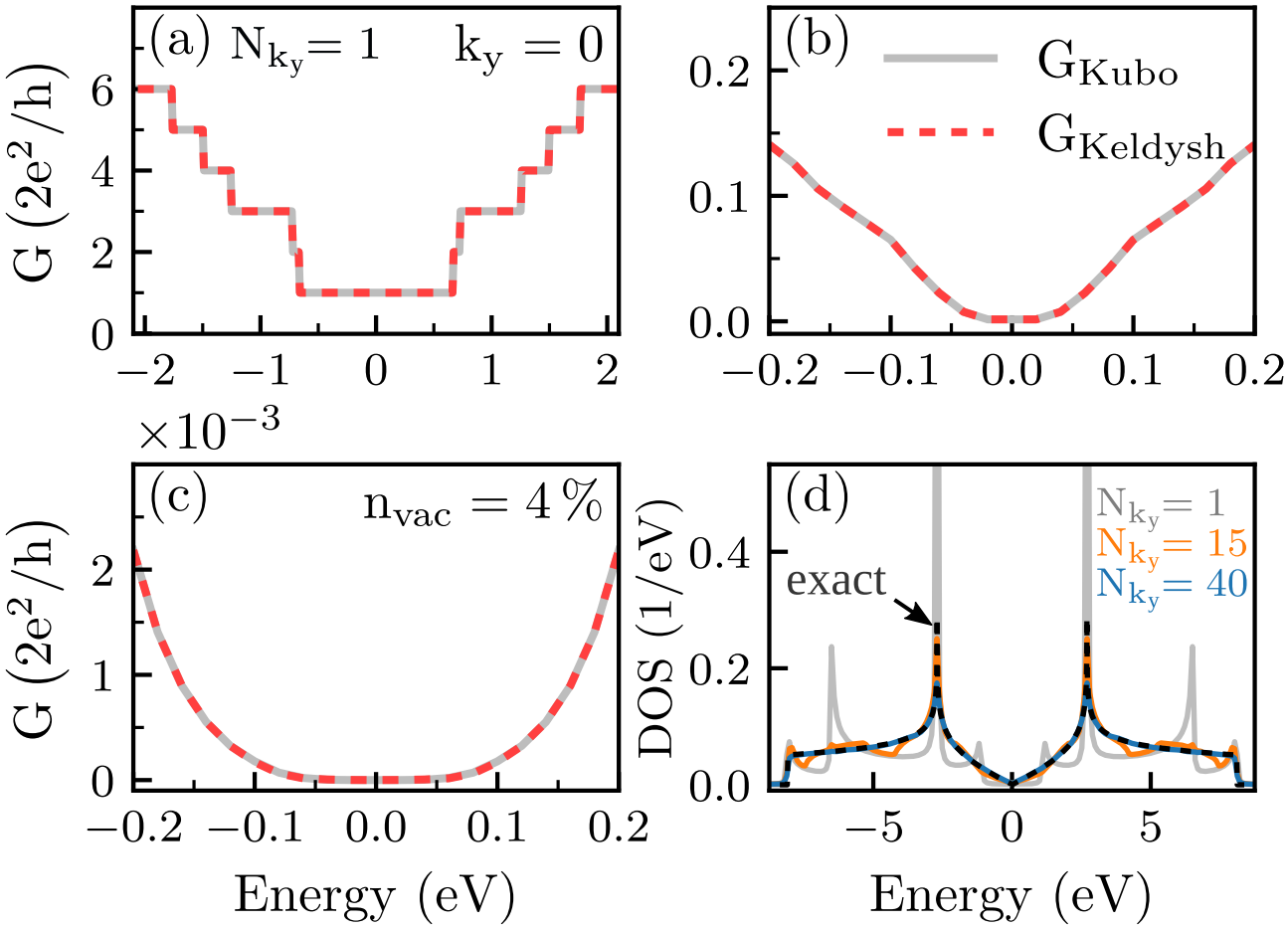

FIG. S1. (a)–(c) Illustration of the well-established [1, 2] equivalence of Keldysh [20] G_{Keldysh} [Eq. (12)] and Kubo [Eq. (11)] G_{Kubo} [1, 12, 21] conductance formulas for the example of an infinite graphene in the two-terminal setup of Fig. 1 of the main text which is clean in (a) and (b) and disordered by vacancies [22] of concentration n_{vac}. In (a) $k_y = 0$, so we use $N_{k_y} = 1$ point, while in (b) we sum [23, 24] over all k_y points using the variable number of k_y points (depending on energy) in an adaptive integration scheme for functions with sharp gradients and cusps [25]. (d) DOS of clean graphene [i.e., the same as studied in panels (a) and (b)] is obtained from retarded GF [Eq. (14)] of CA region in two-terminal setup of Fig. 1 in the main text for different number of sampled k_y points. The exact analytical formula [3] for DOS of infinite graphene is plotted as a black curve in panel (d) for reference.

and nano junctions, originally explained by G_{Keldysh}. Besides the example of equivalence for conductance calculations we provided in Fig. S1, one can find many others like twisted bilayer graphene in Refs. [18, 19] or three-dimensional crystals in Ref. [2].

Let us also recall that historically G_{Kubo} in Eq. (11) dates back to Kubo [21] and Greenwood [12], as the formula for longitudinal *conductivity* expressed in terms of GFs, which was later recast as the formula for *conductance* in two-terminal Landauer setup [1]. The formula for G_{Keldysh} in Eq. (12) was derived by Caroli *et al.* [20] via the Keldysh formalism, and it can also be viewed as the GF-based expression of the Landauer two-terminal conductance formula [1, 15–17]

$$G_{\text{Landauer}} = \frac{2e^2}{h} \text{Tr}\left[\mathbf{t}\mathbf{t}^\dagger\right] \equiv G_{\text{Keldysh}}. \tag{13}$$

Here the transmission matrix $\mathbf{t}$ is connected to GFs quantities via the Fisher-Lee relation [26–29], $\mathbf{t} = \sqrt{\hat{\Gamma}_{\text{R}}} \cdot \hat{G}^r \cdot \sqrt{\hat{\Gamma}_{\text{L}}}$. For spin-dependent transport, one should divide prefactors in Eqs. (11)–(13) by 2.

V. DENSITY OF STATES OF GRAPHENE FROM GREEN'S FUNCTION OF TWO-TERMINAL SETUP IN FIG. 1 IN THE MAIN TEXT

Finally, Fig. S1(d) plots DOS of plain graphene as

$$\mathrm{DOS}(E) = -\frac{W}{2\pi^2}\int_{-\pi/W}^{\pi/W} dk_y\, \mathrm{Tr}\left[\mathrm{Im}\,\hat{G}(E,k_y)\right], \tag{14}$$

using retarded and advanced GFs, $\mathrm{Im}\,\hat{G} = (\hat{G}^r - \hat{G}^a)/2i$, of CA region in two-terminal setup of Fig. 1 in the main text where infinite in longitudinal direction graphene nanoribbon of width W is periodically repeated along the transverse y-direction. By increasing sampling [24] of k_y points, we numerically obtain from Eq. (14) DOS which perfectly matches [Fig. S1(d)] the well-known analytical formula [3] for DOS of infinite graphene. This confirms that our setup in Fig. S1 is capturing the behavior of bulk graphene (as discussed before and used to explain experiments on large graphene sheets [23]), rather than modeling quantum transport in nanowire-based devices.

[1] H. U. Baranger and A. D. Stone, Electrical linear-response theory in an arbitrary magnetic field: A new Fermi-surface formation, Phys. Rev. B **40**, 8169 (1989).
[2] B. K. Nikolić, Deconstructing Kubo formula usage: Exact conductance of a mesoscopic system from weak to strong disorder limit, Phys. Rev. B **64**, 165303 (2001).
[3] A. H. Castro Neto, F. Guinea, N. M. R. Peres, K. S. Novoselov, and A. K. Geim, The electronic properties of graphene, Rev. Mod. Phys. **81**, 109 (2009).
[4] A. Bastin, C. Lewiner, O. Betbeder-matibet, and P. Nozieres, Quantum oscillations of the Hall effect of a fermion gas with random impurity scattering, J. Phys. Chem. Solids **32**, 1811 (1971).
[5] M. Brandbyge, J.-L. Mozos, P. Ordejón, J. Taylor, and K. Stokbro, Density-functional method for nonequilibrium electron transport, Phys. Rev. B **65**, 165401 (2002).
[6] D. A. Areshkin and B. K. Nikolić, Electron density and transport in top-gated graphene nanoribbon devices: First-principles green function algorithms for systems containing a large number of atoms, Phys. Rev. B **81**, 155450 (2010).
[7] F. Freimuth, S. Blügel, and Y. Mokrousov, Spin-orbit torques in Co/Pt(111) and Mn/W(001) magnetic bilayers from first principles, Phys. Rev. B **90**, 174423 (2014).
[8] L. Smrčka and P. Středa, Transport coefficients in strong magnetic fields, J. Phys. C: Solid State Phys. **10**, 2153 (1977).
[9] P. Středa, Theory of quantised Hall conductivity in two dimensions, J. Phys. C: Solid State Phys. **15**, L717 (1982).
[10] T. Ozaki, Continued fraction representation of the Fermi-Dirac function for large-scale electronic structure calculations, Phys. Rev. B **75**, 035123 (2007).
[11] V. Bonbien and A. Manchon, Symmetrized decomposition of the Kubo-Bastin formula, Phys. Rev. B **102**, 085113 (2020).
[12] D. A. Greenwood, The Boltzmann equation in the theory of electrical conduction in metals, Prof. Phys. Soc. London **71**, 585 (1958-04).
[13] G. Stefanucci and R. van Leeuwen, *Nonequilibrium Many-Body Theory of Quantum Systems: A Modern Introduction* (Cambridge University Press, Cambridge, 2013).
[14] Nevertheless, confusion still occasionally appears in the literature, such as in Fig. 6 of Ref. [30] where Kubo approach does not match quantized G_{Keldysh} of an infinite clean wire.
[15] Y. Imry, *Introduction to Mesoscopic Physics* (Oxford University Press, Oxford, 2002).
[16] Y. Imry and R. Landauer, Conductance viewed as transmission, Rev. Mod. Phys. **71**, S306 (1999).
[17] Y. V. Nazarov and Y. M. Blanter, *Quantum Transport: Introduction to Nanoscience* (Cambridge University Press, Cambridge, 2009).
[18] S. G. de Castro, A. Ferreira, and D. A. Bahamon, Efficient Chebyshev polynomial approach to quantum conductance calculations: Application to twisted bilayer graphene, Phys. Rev. B **107**, 045418 (2023).
[19] S. G. de Castro, J. a. M. V. P. Lopes, A. Ferreira, and D. A. Bahamon, Fast Fourier-Chebyshev approach to real-space simulations of the Kubo formula, Phys. Rev. Lett. **132**, 076302 (2024).
[20] C. Caroli, R. Combescot, P. Nozieres, and D. Saint-James, Direct calculation of the tunneling current, J. Phys. C: Solid State Phys. **4**, 916 (1971).
[21] R. Kubo, Statistical-mechanical theory of irreversible processes. I. general theory and simple applications to magnetic and conduction problems, J. Phys. Soc. Jpn. **12**, 570 (1957).
[22] A. Ferreira and E. R. Mucciolo, Critical delocalization of chiral zero energy modes in graphene, Phys. Rev. Lett. **115**, 106601 (2015).
[23] M.-H. Liu and K. Richter, Efficient quantum transport simulation for bulk graphene heterojunctions, Phys. Rev. B **86**, 115455 (2012).
[24] K. S. Thygesen and K. W. Jacobsen, Interference and k-point sampling in the supercell approach to phase-coherent transport, Phys. Rev. B **72**, 033401 (2005).

[25] S. Mousavi, J. Pask, and N. Sukumar, Efficient adaptive integration of functions with sharp gradients and cusps in n-dimensional parallelepipeds, Int. J. Numer. Methods Eng. **91**, 343 (2012).
[26] D. S. Fisher and P. A. Lee, Relation between conductivity and transmission matrix, Phys. Rev. B **23**, 6851 (1981).
[27] T. Ando, Quantum point contacts in magnetic fields, Phys. Rev. B **44**, 8017 (1991).
[28] P. A. Khomyakov, G. Brocks, V. Karpan, M. Zwierzycki, and P. J. Kelly, Conductance calculations for quantum wires and interfaces: Mode matching and green's functions, Phys. Rev. B **72**, 035450 (2005).
[29] X. Waintal, M. Wimmer, A. Akhmerov, C. Groth, B. K. Nikolić, M. Istas, T. Örn Rosdahl, and D. Varjas, Computational quantum transport, arXiv:2407.16257 (2024).
[30] Z. Fan, J. H. Garcia, A. W. Cummings, J. E. Barrios-Vargas, M. Panhans, A. Harju, F. Ortmann, and S. Roche, Linear scaling quantum transport methodologies, Phys. Rep. **903**, 1 (2021).